ChemComm

Check for updates

Thermochemically stable ceramic composite membranes based on Bi₂O₃ for oxygen separation with high permeability†

Wen Xing, [iD] * Patricia A. Carvalho, Jonathan M. Polfus [iD] and Zuoan Li

Ceramic oxygen separation membranes can be utilized to reduce CO_2 emissions in fossil fuel power generation cycles based on oxy-fuel combustion. State-of-the-art oxygen permeable membranes based on $Ba_{0.5}Sr_{0.5}Co_{0.8}Fe_{0.2}O_{3-\delta}$ (BSCF) offer high oxygen permeability but suffer from long-term instability, especially in the presence of CO_2. In this work, we present a novel ceramic composite membrane consisting of 60 vol% $(Bi_{0.8}Tm_{0.2})_2O_{3-\delta}$ (BTM) and 40 vol% $(La_{0.8}Sr_{0.2})_{0.99}MnO_{3-\delta}$ (LSM), which shows not only comparable oxygen permeability to that of BSCF but also outstanding long-term stability. At 900 °C, oxygen fluxes of 1.01 mL min^{-1} cm^{-2} and 1.33 mL min^{-1} cm^{-2} were obtained for membranes with thicknesses of 1.35 mm and 0.75 mm, respectively. Moreover, significant oxygen fluxes were obtained at temperatures down to 600 °C. A stable operation of the membrane was demonstrated with insignificant changes in the oxygen flux at 750 °C for approx. one month and at 700 °C with 50% CO_2 as the sweep gas for more than two weeks.

Dense ceramic oxygen permeable membranes can separate oxygen from air at temperatures above 600 °C with higher energy efficiency than that in cryogenic distillation or pressure swing adsorption, especially when thermally and/or chemically integrated in high temperature processes.[1] The separated oxygen can be used for gasification of coal and biomass, and in oxy-fuel combustion processes for power generation with carbon capture.[2] Besides their applications in the energy sector, ceramic oxygen permeable membranes can also be used in small scale oxygen production or catalytic membrane reactors for the partial oxidation of methane to syngas, and for the production of chemicals.[3,4] It is particularly beneficial with chemical integration of the membranes which then must be CO_2-tolerant for most applications, *e.g.*, oxy-fuel with recirculated flue gas on the permeate side.[5]

Dense ceramic membranes rely on the ambipolar transport of both oxide ions and electrons or holes, *i.e.*, mixed ionic and electronic conduction (MIEC). The highest oxygen permeation

rates for this type of mixed conducting membranes were found in $Ba_{1-x}Sr_xFeO_{3-\delta}$ and $SrCo_{1-x}Fe_xO_{3-\delta}$ based perovskites such as $Ba_{0.5}Sr_{0.5}Co_{0.8}Fe_{0.2}O_{3-\delta}$ (BSCF). The oxygen flux of asymmetric and thin BSCF membranes can reach ~10 mL min^{-1} cm^{-2}.[6,7] However, BSCF suffers from several structural and chemical instability issues that hinder the material's practical application as membranes. BSCF undergoes a phase transition from cubic to hexagonal that leads to its decomposition into two phases when annealed below 850 °C.[8–10] Due to the basicity of barium, BSCF exhibits severe reactivity towards CO_2 which significantly reduces the membrane performance.[11] The high thermal expansion coefficient of BSCF (approx. 20×10^{-6} K^{-1}) also limits its integration with other components in modules or reactors.[12] Membrane materials that are stable towards CO_2 such as $SrFe_{0.9}Ta_{0.1}O_{3-\delta}$[13] and $(Pr_{0.9}La_{0.1})_2(Ni_{0.74}Cu_{0.21}Ga_{0.05})O_{4+\delta}Cl_{0.1}$[14] exhibit lower oxygen fluxes of 0.3 and 0.8 mL min^{-1} cm^{-2} at 900 °C for disc membranes of 1 mm and 0.6 mm thicknesses, respectively, as compared to BSCF.

Ambipolar transport of oxide ions and electrons can alternatively be achieved by means of a ceramic composite comprising an oxide ion conducting electrolyte and an electronic conducting oxide. Chemical compatibility between the phases is crucial, and the interphase between the two materials plays an important role in determining the membrane performance and stability. For instance, segregation or reaction along the heterophase boundaries may lead to the formation of blocking phases that limit the overall oxide ion and/or electronic transport, while sufficient adherence between the phases is required.

The ambipolar conductivity and oxygen flux of the composite membranes is usually limited by the oxide ion conducting phase since the conductivity of a percolating electronic conducting phase can be significantly higher. Fluorite structured oxides have been selected due to their excellent chemical stability and relatively high oxide ion conductivity. Composites of acceptor doped CeO_2 with electronic or mixed conducting oxides have been extensively studied, and present moderate oxygen fluxes as compared to BSCF with a similar thickness.[15–26] Composite membranes based on stabilised ZrO_2 show even lower oxygen fluxes.[27–29]

SINTEF Industry, Sustainable Energy Technology, Pb. 124 Blindern, 0314 Oslo, Norway. E-mail: wen.xing@sintef.no

† Electronic supplementary information (ESI) available. See DOI: 10.1039/c8cc10077b

In comparison to CeO_2 and ZrO_2 based oxide ion conductors, δ-Bi_2O_3 shows a higher oxide ion conductivity[30] and the high temperature phase can be stabilized at lower temperatures by doping with lanthanide elements.[31–34] Previous studies have focused on composite membranes based on doped Bi_2O_3 mixed with noble metals and relatively high oxygen fluxes were obtained.[35–37] However, these cermet membranes exhibited high and unsuitable thermal expansion, and the use of noble metals may be an issue for their applicability due to the material cost.

Here we present a composite oxygen separation membrane based on Tm-doped Bi_2O_3 and p-type conducting Sr-doped $LaMnO_3$. Among the lanthanide dopants for Bi_2O_3, thulium was chosen due to its suitable ionic radius for attaining the cubic δ-Bi_2O_3 phase which exhibits high phase stability at lower temperatures and high oxide ion conductivity.[34]

The composite pellet membranes were synthesized by the solid-state reaction method. Bi_2O_3 (99.9%, Sigma Aldrich) and 20 molar percent of Tm_2O_3 (99.9%, Sigma Aldrich) were weighed and mixed in an agate mortar. The mixture was calcinated at 750 °C for 10 hours to form a single phase $(Bi_{0.8}Tm_{0.2})_2O_{3-\delta}$. $(La_{0.8}Sr_{0.2})_{0.99}MnO_{3-\delta}$ (LSM) was synthesized by spray pyrolysis (Cerpotech, Norway). The BTM and LSM powders were mixed in an agate mortar with a volume ratio of 60% to 40%, respectively, to ensure percolation of both phases. Green pellets ($\varnothing$ = 21 mm) were pressed and sintered at 1000 °C for 10 hours resulting in membranes with a relative density of 93%. The samples were characterised by scanning electron microscopy (SEM) using an FEI Nova NaonSEM 650 apparatus. Phase boundary observations were carried out by scanning transmission electron microscopy (STEM) using a DCOR Cs probe-corrected FEI Titan G2 60-300 instrument with 0.08 nm of nominal spatial resolution (details can be found in ESI†). The thermal expansion coefficient of the composite membrane was measured using a NETZSCH Dilatometer 402E.

The disc samples were polished using an SiC paper down to 2 μm roughness. Gold ring sealing gaskets of 13 mm in diameter were polished using a diamond paste down to 250 nm roughness. The samples were mounted in a ProboStat measurement cell (NORECS, Norway) and sealed to an alumina riser tube upon heating the setup to 950 °C. The He leakage to the sweep was monitored by gas chromatography (GC, Varian CP-4900) using helium and oxygen mixtures as feed gases. Throughout the measurements after the sealing was achieved, no helium was detected in the sweep gas stream within the detection limit of the GC (1 ppm). Therefore, the oxygen flux (j_{O_2}) was obtained from the concentration of oxygen measured by GC in the sweep (c_{O_2}) according to the following equation:

$$j_{O_2} = c_{O_2}F_{sweep}/A \qquad (1)$$

where F_{sweep} is the sweep flow rate in mL min^{-1} and A is the membrane surface area in cm^2.

The SEM cross-section images shown in Fig. 1 show dark LSM grains immersed in large grained BTM, forming interconnected networks. The grain growth of LSM can be observed after the permeation test for about 2 months, and no secondary phases were observed by XRD (Fig. S5, ESI†).
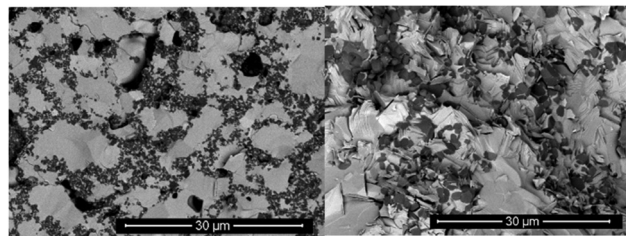

Fig. 1 Fracture cross-section of the composite membrane before (left) and after (right) a long term flux test by SEM. The darker grains are LSM and the brighter phase is BTM.

The detailed structural and chemical properties of the interface between BTM and LSM were investigated by STEM. The observations revealed high interfacial adhesion (Fig. 2(a)), and EDS line profiles across the interfaces showed a substantial cation interdiffusion within about 40 nm (Fig. 2(b)). Fig. 2(c) shows that the interfaces were atomically smooth and coherent, which can be ascribed to the similar interatomic distances in the two structures (see XRD patterns in ESI†). The atomic resolution EDS mapping confirms the La substitution by Sr in the LSM phase (Fig. 2(d)), while no chemical segregation at the interfaces from either BTM or LSM could be detected (see Fig. 2(e)). The pristine interfaces in the composite observed by TEM may enhance an interfacial oxide ion diffusion in LSM as reported recently.[38]
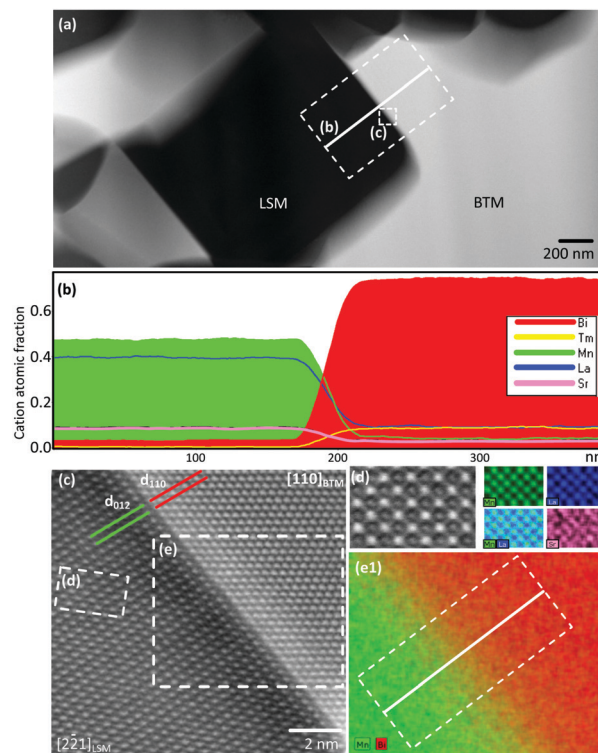

Fig. 2 (a) HAADF image of the interface between two grains of LSM (darker) and BTM (brighter). (b) Elemental profile across the interface along the line drawn in (a) averaged through the dashed area. (c) High-resolution HAADF image of the interface. (d) Detail of (c) with the corresponding EDS maps of La, Mn and Sr. (e1) Overlapping EDS maps of Mn and Bi corresponding to the detail (e).

Fig. 3 shows the measured oxygen fluxes of the BTM–LSM membranes with different thicknesses as a function of inverse temperature in comparison to the literature data for BSCF and composites based on the acceptor-doped CeO_2 and ZrO_2 with similar thicknesses. At high temperatures, the thinner 0.75 mm membrane shows a higher oxygen flux than the thicker 1.35 mm membrane. The oxygen fluxes were similar at temperatures below 750 °C, which indicate limiting surface kinetics at lower temperatures.‡ Overall, the BTM–LSM composite membranes show a comparable oxygen flux to that of the BSCF membranes and a higher oxygen flux than the CeO_2 and ZrO_2 based composite membranes that can be ascribed to the higher oxide ion conductivity in the acceptor-doped Bi_2O_3.

Based on Wagner transport theory for mixed conducting membranes and assuming no surface kinetics limitations, the oxygen flux is proportional to the chemical potential gradient of oxygen across the membrane:

$$j_{O_2} \propto RT \log\left(\frac{P_{O_2}^{feed}}{P_{O_2}^{sweep}}\right) \qquad (2)$$

In this respect, it was found that increasing the flow from 120 mL min^{-1} on the feed side containing 50% O_2 did not influence the oxygen flux. The flow was therefore sufficient to avoid concentration polarization on the feed side of the membranes. On the other hand, a significant increase in the oxygen flux was obtained by increasing the argon sweep flow rate from 30 mL min^{-1} to 480 mL min^{-1} (Fig. 4). At 900 °C, the measured oxygen flux increased by more than 50% from the lowest to the highest sweep flow due to the higher oxygen gradient (eqn (2)),§ while the improvement was less pronounced at lower temperatures.

The long-term flux stability of the BTM–LSM membranes was investigated for up to 1 month at 750 °C and with 50% CO_2 in the sweep for more than 400 hours at 700 °C. First, the O_2 flux was essentially unchanged with 50% CO_2 in the sweep throughout 900 °C to 600 °C (Fig. S4, ESI†). Subsequently, the
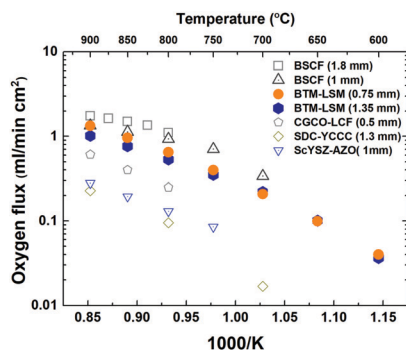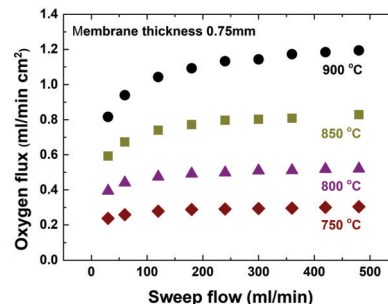

Fig. 4 Oxygen flux of BTM–LSM as a function of the sweep flow rate at different temperatures.

membrane was kept with 50% CO_2 in the sweep at 700 °C, and Fig. 5 shows that the flux exhibited a moderate decrease of about 10% during the initial 100 hours, while it remained stable for the remaining 300 hours. Finally, the flux was measured at 750 °C with argon sweep for about 700 hours where the membrane showed very good stability with insignificant changes in the oxygen flux. Carbonate formation was not observed by SEM or XRD (Fig. S5, ESI†).

The thermal expansion coefficient of BTM–LSM at temperatures between 300 °C and 900 °C in air was 12.5×10^{-6} °C^{-1} upon heating and 11.5×10^{-6} °C^{-1} during cooling. BTM–LSM composite membranes thereby show significantly lower thermal expansion than BSCF which is crucial for system integration of the membranes in reactors or modules.

Further improvements in the oxygen permeation performance of the BTM–LSM system may be achieved by optimization of the

Fig. 3 Oxygen flux as a function of inverse temperature for the BTM–LSM compared to BSCF and acceptor-doped CeO_2 and ZrO_2 composite membranes. The oxygen content in the feed gas was normalised to 50%. Flux data was included for BSCF membranes with thicknesses of 1.8 mm[10] and 1 mm,[39] composites of $Ce_{0.85}Gd_{0.1}Cu_{0.05}O_{2-\delta}$ (CGCO) and $La_{0.6}Ca_{0.4}FeO_{3-\delta}$ (LCF),[21] $Sm_{0.2}Ce_{0.8}O_{1.9-\delta}$ (SDC) and $Y_{0.8}Ca_{0.2}Cr_{0.8}Co_{0.2}O_{3-\delta}$ (YCCC),[23] and $(ZrO_2)_{0.89}(Y_2O_3)_{0.01}(Sc_2O_3)_{0.10}$ (ScYSZ) and $Al_{0.02}Zn_{0.98}O_{1.01}$ (AZO).[29]
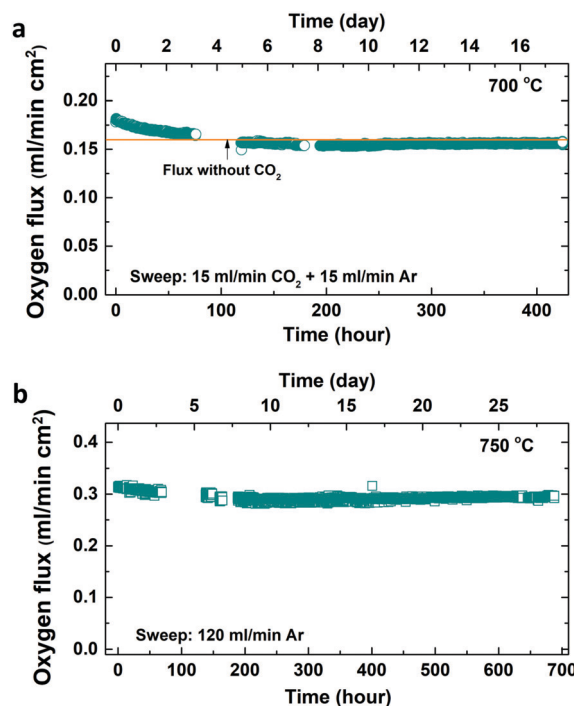

Fig. 5 (a) Oxygen flux with 50% CO_2 sweep at 700 °C for more than 400 hours and (b) subsequently at 750 °C with Ar sweep for approximately one month.

Bi$_2$O$_3$ dopant and microstructure of the composite, while supported asymmetric membrane architectures with catalytic layers should be pursued for the future membrane development.

Ceramic composite membranes based on oxide ion conducting Tm-doped Bi$_2$O$_3$ and the p-type conducting Sr-doped LaMnO$_3$ exhibit good chemical compatibility and comparable oxygen permeation rates compared to BSCF. Moreover, the BTM–LSM membranes show excellent stability at working temperatures in the presence of CO$_2$ containing atmospheres. The thermal expansion coefficient of the composite is significantly lower than that of BSCF, and suitable for integration with other components. Overall, composite membranes based on BTM–LSM are outstanding in many aspects compared to the current state-of-the-art material systems, and may support the future use of the ceramic oxygen separation membrane in clean energy applications.

Conflicts of interest

There are no conflicts to declare.

Notes and references

‡ Additional evidence of limiting surface kinetics can be found in Fig. S2 in the ESI.†
§ The membrane performance does not follow exactly eqn (2) as surface kinetics plays an important role in this case. A plot of the oxygen fluxes as a function of oxygen partial pressure gradient can be found in Fig. S3 in the ESI.†

1 C. Zhang, J. Sunarso and S. Liu, *Chem. Soc. Rev.*, 2017, **46**, 2941–3005.
2 R. Kneer, D. Toporov, M. Forster, D. Christ, C. Broeckmann, E. Pfaff, M. Zwick, S. Engels and M. Modigell, *Energy Environ. Sci.*, 2010, **3**, 198–207.
3 A. Thursfield and I. S. Metcalfe, *J. Mater. Chem.*, 2004, **14**, 2475–2485.
4 S. S. Hashim, A. R. Mohamed and S. Bhatia, *Renewable Sustainable Energy Rev.*, 2011, **15**, 1284–1293.
5 M. A. Habib, H. M. Badr, S. F. Ahmed, R. Ben-Mansour, K. Mezghani, S. Imashuku, G. J. la O', Y. Shao-Horn, N. D. Mancini, A. Mitsos, P. Kirchen and A. F. Ghoneim, *Int. J. Energy Res.*, 2011, **35**, 741–764.
6 X. Zhu, S. Sun, Y. Cong and W. Yang, *J. Membr. Sci.*, 2009, **345**, 47–52.
7 S. Baumann, J. M. Serra, M. P. Lobera, S. Escolástico, F. Schulze-Küppers and W. A. Meulenberg, *J. Membr. Sci.*, 2011, **377**, 198–205.
8 S. Švarcová, K. Wiik, J. Tolchard, H. J. M. Bouwmeester and T. Grande, *Solid State Ionics*, 2008, **178**, 1787–1791.
9 M. Arnold, T. M. Gesing, J. Martynczuk and A. Feldhoff, *Chem. Mater.*, 2008, **20**, 5851–5858.
10 Z. Shao, W. Yang, Y. Cong, H. Dong, J. Tong and G. Xiong, *J. Membr. Sci.*, 2000, **172**, 177–188.
11 M. Arnold, H. Wang and A. Feldhoff, *J. Membr. Sci.*, 2007, **293**, 44–52.
12 S. McIntosh, J. F. Vente, W. G. Haije, D. H. A. Blank and H. J. M. Bouwmeester, *Chem. Mater.*, 2006, **18**, 2187–2193.
13 J. Zhu, S. Guo, Z. Chu and W. Jin, *J. Mater. Chem. A*, 2015, **3**, 22564–22573.
14 J. Xue, J. Li, L. Zhuang, L. Chen, A. Feldhoff and H. Wang, *Chem. Eng. J.*, 2018, **347**, 84–90.
15 V. V. Kharton, A. V. Kovalevsky, A. P. Viskup, A. L. Shaula, F. M. Figueiredo, E. N. Naumovich and F. M. B. Marques, *Solid State Ionics*, 2003, **160**, 247–258.
16 A. J. Samson, M. Søgaard and P. Vang Hendriksen, *J. Membr. Sci.*, 2014, **470**, 178–188.
17 X. F. Zhu and W. S. Yang, *AIChE J.*, 2008, **54**, 665–672.
18 T. Chen, H. Zhao, N. Xu, Y. Li, X. Lu, W. Ding and F. Li, *J. Membr. Sci.*, 2011, **370**, 158–165.
19 Y. Lin, S. Fang, D. Su, K. S. Brinkman and F. Chen, *Nat. Commun.*, 2015, **6**, 6824.
20 S. Cheng, M. Sogaard, L. Han, W. Zhang, M. Chen, A. Kaiser and P. V. Hendriksen, *Chem. Commun.*, 2015, **51**, 7140–7143.
21 W. Fang, F. Liang, Z. Cao, F. Steinbach and A. Feldhoff, *Angew. Chem., Int. Ed.*, 2015, **54**, 4847–4850.
22 S. Fang, C. Chen and L. Winnubst, *Solid State Ionics*, 2011, **190**, 46–52.
23 K. J. Yoon and O. A. Marina, *J. Membr. Sci.*, 2016, **499**, 301–306.
24 K. Partovi, C. H. Rüscher, F. Steinbach and J. Caro, *J. Membr. Sci.*, 2016, **503**, 158–165.
25 H. Li, Y. Liu, X. Zhu, Y. Cong, S. Xu, W. Xu and W. Yang, *Sep. Purif. Technol.*, 2013, **114**, 31–37.
26 H. Luo, H. Jiang, T. Klande, F. Liang, Z. Cao, H. Wang and J. Caro, *J. Membr. Sci.*, 2012, **423–424**, 450–458.
27 S. Lia, W. Jin, N. Xu and J. Shi, *J. Membr. Sci.*, 2001, **186**, 195–204.
28 W. He, H. Huang, J.-F. Gao, L. Winnubst and C.-S. Chen, *J. Membr. Sci.*, 2014, **452**, 294–299.
29 S. Pirou, J. M. Bermudez, P. V. Hendriksen, A. Kaiser, T. R. Reina, M. Millan and R. Kiebach, *J. Membr. Sci.*, 2017, **543**, 18–27.
30 P. Shuk, H. D. Wiemhöfer, U. Guth, W. Göpel and M. Greenblatt, *Solid State Ionics*, 1996, **89**, 179–196.
31 H. T. Cahen, T. G. M. Van Den Belt, J. H. W. De Wit and G. H. J. Broers, *Solid State Ionics*, 1980, **1**, 411–423.
32 S. Boyapati, E. D. Wachsman and N. Jiang, *Solid State Ionics*, 2001, **140**, 149–160.
33 M. Drache, P. Roussel and J.-P. Wignacourt, *Chem. Rev.*, 2007, **107**, 80–96.
34 A. Dapčević, D. Poleti, J. Rogan, A. Radojković, M. Radović and G. Branković, *Solid State Ionics*, 2015, **280**, 18–23.
35 J. Kim and Y. S. Lin, *J. Membr. Sci.*, 2000, **167**, 123–133.
36 K. Kobayashi and T. Tsunoda, *Solid State Ionics*, 2004, **175**, 405–408.
37 K. Wu, S. Xie, G. S. Jiang, W. Liu and C. S. Chen, *J. Membr. Sci.*, 2001, **188**, 189–193.
38 J. M. Polfus, B. Yildiz and H. L. Tuller, *Phys. Chem. Chem. Phys.*, 2018, **20**, 19142–19150.
39 S. Baumann, F. Schulze-Küppers, S. Roitsch, M. Betz, M. Zwick, E. M. Pfaff, W. A. Meulenberg, J. Mayer and D. Stöver, *J. Membr. Sci.*, 2010, **359**, 102–109.